International Journal of Materials Science
ISSN 0973-4589 Volume 12, Number 1 (2017), pp. 137-147

http://www.ripublication.com

Structural, electronic, optical and mechanical properties of $CsCaCl_3$ and $KCdF_3$ cubic perovskites

Madan Lal[1] [2*] and Shikha Kapila[3]

[1]Department of Physics, Govt Degree College Una, Himachal Pradesh-174303 (India)
[2]Research Scholar,I.K.Gujral Punjab Technical University, Jalandhar Punjab -144603 (India)
[3]Department of Applied Science, Bahra Group of Institutions, Bhedpura Patiala Punjab -147001 (India)

Abstract

First principles studies are performed on the structural, electronic, optical and mechanical properties of the cubic perovskites $CsCaCl_3$ and $KCdF_3$. The Kohn–Sham equations are solved by applying the full potential linearized augmented plane wave (FP-LAPW) method. The exchange correlation effects are included through the local density approximation (LDA), generalized gradient approximation (GGA) and modified Becke-Johnson (mBJ) exchange potential. The calculated lattice constant is in good agreement with the experimental result. The calculations of electronic band structure and density of states show that these compounds have indirect energy band gap (M-Γ) with a mixed ionic and covalent bonding. Calculations of the optical spectra such as the real and imaginary parts of dielectric function, reflectivity, photoconductivity and refractive index are performed.

Keywords: lattice constants, bulk modulus, band gap, perovskites

1. INTRODUCTION

Perovskite (ABX_3) is one of the most frequently encountered structures in solid-state physics, and it accommodates most of the metallic ions in the periodic table with a significant number of different anions. However, there are very few studies that have focused on the evolution of the bonding mechanism of ferroelectric perovskite

materials according to the lattice distortions. Among the perovskite oxides studied most intensively are zirconates of alkaline earth metals. Indeed, they are currently gaining considerable importance in the field of electrical ceramics, refractories, geophysics, astrophysics, particle accelerators, fission, fusion reactors, heterogeneous catalysis etc. Additionally, they have received great attention as high temperature proton conductors with the possibility of applications in fuel cells or hydrogen sensors [1,2].

Although majority of the perovskite compounds are oxides or fluorides, other forms like heavier halides, sulphides, hydrides, cyanides, oxyfluorides and oxynitrides are also reported [3-5]. Oxide perovskites are popular in major industrial applications due to their diverse physical properties [5] over a wide temperature range. Above the Curie temperature, most of them have ideal cubic crystal structure. As the temperature is lowered, they transform from the high-symmetry para electric phase to slightly distorted ferroelectric structures with tetragonal, orthorhombic and rhombohedral symmetries. Typically, the phase transitions are characterized by a small macroscopic lattice strain and microscopic displacement of ions [6-10]. A large number of the perovskites undergo a series of the structural phase transitions ranging from nonpolar antiferrodistortive to ferroelectric to antiferroelectric in nature as temperature is reduced. These transitions are an outcome of the delicate balance between long-range dipole–dipole interactions that favor the ferroelectric state and short-range forces that favor the cubic perovskite phase [11]. These structural phase transitions involve very small atomic displacements away from the ideal cubic structure and the energy differences are small. First principles density functional calculations have significant success in providing accurate total-energy surfaces for the perovskites to explain the ferroelectric distortions [8,12].

Moreover, neither experimental nor theoretical efforts have been made to explore electronic and optical properties of these ternary oxides. With this motivation, we perform density functional theory (DFT) calculations to prove structural, electronic optical and mechanical properties of $CsCaCl_3$ and $KCdF_3$ cubic perovskites.

2. COMPUTATIONAL METHODS

The calculations were done using FP-LAPW computational scheme [13,14] as implemented in the WIEN2K code [15]. The FP-LAPW method expands the Kohn-Sham orbitals in atomic like orbitals inside the muffin-tin (MT) atomic spheres and plane waves in the interstitial region. The Kohn-Sham equations were solved using the recently developed Wu-Cohen generalized gradient approximation (WC-GGA) [16, 17] for the exchange-correlation (XC) potential. It has been shown that this new functional is more accurate for solids than any existing GGA and meta-GGA forms. For a variety of materials, it improves the equilibrium lattice constants and bulk moduli significantly over local-density approximation [18] and Perdew-Burke-Ernzerhof (PBE) [19] and therefore is a better choice. For this reason we adopted the new WC approximation for the XC potential in studying the present systems. Further

for electronic structure calculations modified Becke–Johnson potential (mBJ) [20] as coupled with WC-GGA is used.

The valence wave functions inside the atomic spheres were expanded up to l=10 partial waves. In the interstitial region, a plane wave expansion with $R_{MT}K_{max}$ = 7 was used for all the investigated systems, where R_{MT} is the minimum radius of the muffin-tin spheres and K_{max} gives the magnitude of the largest K vector in the plane wave expansion. The potential and the charge density were Fourier expanded up to G_{max} = 12. We carried out convergence tests for the charge-density Fourier expansion using higher G_{max} values. The modified tetrahedron method [20] was applied to integrate inside the Brillouin zone (BZ) with a dense mesh of 5000 uniformly distributed k-points (equivalent to 405 in irreducible BZ) where the total energy converges to less than 10^{-6} Ry.

3. RESULTS AND DISCUSSION

3.1 Structural properties

ABX_3 (A = Cs, K; B = Ca, Cd; X = F, Cl) crystallize in cubic structure having space group Pm3m (#221). The A, B and X atoms are positioned at (0 0 0), (1/2, 1/2,1/2), (1/2, 1/2, 0) sites of Wyckoff coordinates respectively. Energy versus volume minimization process [21] is used to calculate equilibrium lattice parameters such as lattice constants (a_o), ground state energy (E_o), bulk modulus (B), and its pressure derivative (B') by LDA and GGA exchange correlation schemes as shown in Table (1).

Table 1. Structural parameters, lattice constants a (Å), ground state energies E_o (Ry) bulk modulus B (GPa) and its pressure derivative B′ (GPa) with experimental and other theoretical values of $CsCaCl_3$ and $KCdF_3$ cubic perovskites.

Structural analysis	a (Å)	a (Å) exp. [1]	E_o (Ry)	B′	B (GPa)	B (GPa) [1]
$CsCaCl_3$	5.37 (GGA), 5.25 (LDA)	5.39	-19711.201 (GGA), -19688.001 (LDA)	4.51 (GGA), 4.72 (LDA)	23 (GGA), 32 (LDA)	23, 28
$KCdF_3$	4.39 (GGA), 4.31 (LDA)	4.29	-12987.502 (GGA), -12980.052 (LDA)	4.27 (GGA), 5.27 (LDA)	66 (GGA), 74 (LDA)	63

In addition to it, we use lattice parameters calculated by generalized gradient approximation (GGA) for investigating electronic and optical properties.

We can also provide a prediction of the bulk modulus by using the semi-empirical equation developed by Verma et al [1]

$$B\,(GPa) = S + V\frac{(Z_a Z_b Z_c)^{0.35}}{a^{3.5}} \quad (1)$$

where Z_a,, Z_b and Z_c are the ionic charges on the A, B and X, respectively and a is lattice parameter in Å. The S and V are constants and the values are 1.79 and 5505.785 respectively.

3.2 Electronic Properties

The electronic properties of herein investigated perovskites are based on energy band structure and total as well as partial density of states (TDOS and PDOS) while influence of bonding nature is discussed in terms of charge density distribution. Graphically, we have highlight recently improved Trans-Blaha modified Becke–Johnson (TB-mBJ) potential, which removes wrong interpretation of the true unoccupied states of the system which causes underestimation of electronic band gap [22]. The calculated band structures are shown in Figure (1a) and 1(b) for $CsCaCl_3$ and $KCdF_3$ respectively. The calculated values of the band gaps for $CsCaCl_3$ are found to be equal to 5.30, 5.39 and 6.89 eV using LDA, GGA, and mBJ, respectively. The calculated values of the band gaps for $KCdF_3$ are found to be equal to 2.99 eV, 3.08 eV, and 6.85 eV by using LDA, GGA and mBJ, respectively. It is observed that overall trend of band dispersion curves are almost same but conduction band minimum (CBM) lies at Γ and valence band maximum (VBM) lies at M symmetry point of brillouin zone (BZ) revealing (M-Γ) indirect band gap of 6.89 eV and 6.85 eV for $CsCaCl_3$ and $KCdF_3$ compounds respectively.

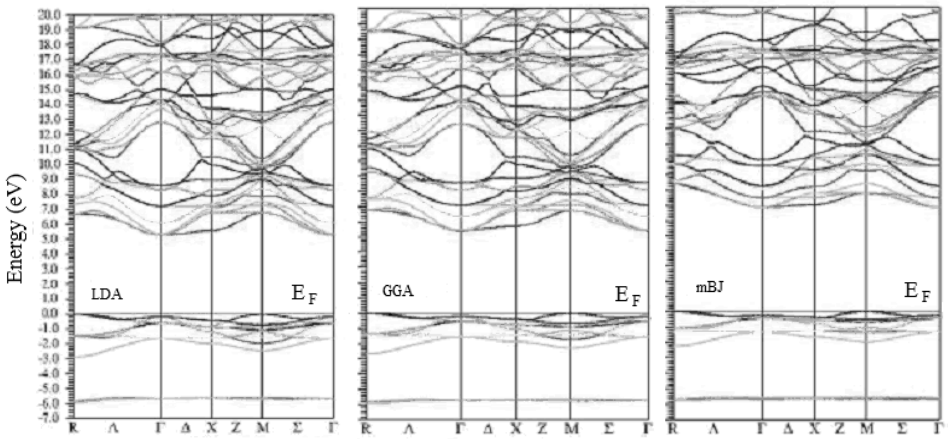

(a)

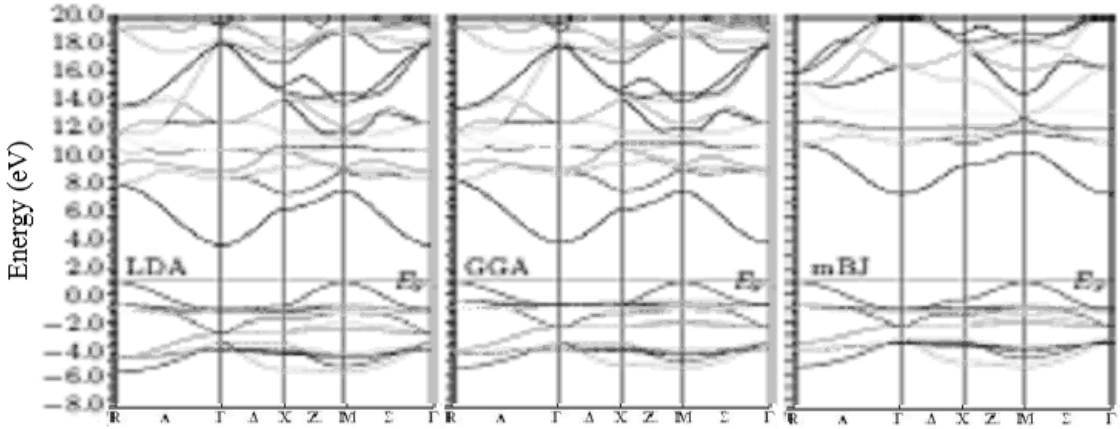

(b)

Figure 1. Band Structure of (a) $CsCdCl_3$ and (b) $KCdF_3$.

On the basis of different bands; the total density of states (TDOS) could be grouped into four regions and the contribution of different states in these bands can be seen from the partial density of states (PDOS). The first region around -5.8 eV comprising a narrow band due to the Cs 5p state is clearly seen from Fig. 2.1 (b). In the second region around -2.75 eV to the Fermi energy level, majority contribution is due to Cl 3p states in Fig. 2.1 (d) and minority contribution is due to Ca 3d states. There is hybridization between Ca 3d with Cl 3p states in this region. The first and second regions within the range of -6:0 to 0 eV comprise the valence band. The upper part of the valence band is composed of the Cl 3p and Ca 3d states. The third region above the Fermi level is the conduction band. The lower part of this band near the Fermi level is mainly due to the contributions from Cl 3p, Cl 3s, and Ca 3p states. In the conduction band from 7.0 eV to 10 eV majority contribution is from Ca 3d states. Along with this majority contribution from Ca 3d states, there are minor contributions from Cs 5d and Cl 2p states observed. From 10 to 20 eV a small contribution is due to the Cs 4f, Cl 3d, Ca 3d, and Cs 5d states in the conduction band. From Fig. 2.2 (b) for $KCdF_3$, it is seen that the TDOS of the compound can be grouped into different regions within energy range −7 eV to 20 eV. The narrow band around −5 eV is due to Cd 4*d* states contribution observed. From −3 eV to the Fermi level, the bands have major contribution of F 2*p* states and minor contribution of Cd 4*d* states. There is hybridization between Cd 4*d* with F 2*p* states in this region. Above the Fermi level, the conduction band minimum (CBM) is composed by Cd 5*s* states. From 10 eV to 14 eV, majority contribution is due to K 3*d* states. The occupied states correspond to the valence band, where the unoccupied states are related to the conduction band. In the present case the K 3*p* states are occupied and K 3*d* states are unoccupied. Therefore the majority contribution comes from K 3*d* states rather than K 3*p* states in the conduction band. From 14 eV to 20 eV, along with K 3*d* states a minor contribution of Cd 4*f* states is observed. These calculations have been measured theoretically and experimentally for $CsCaCl_3$ and $KCdF_3$ by Babu et al. [23, 24] and Macdonald et al

[25] respectively. Our theoretical calculations are in good agreement with their results.

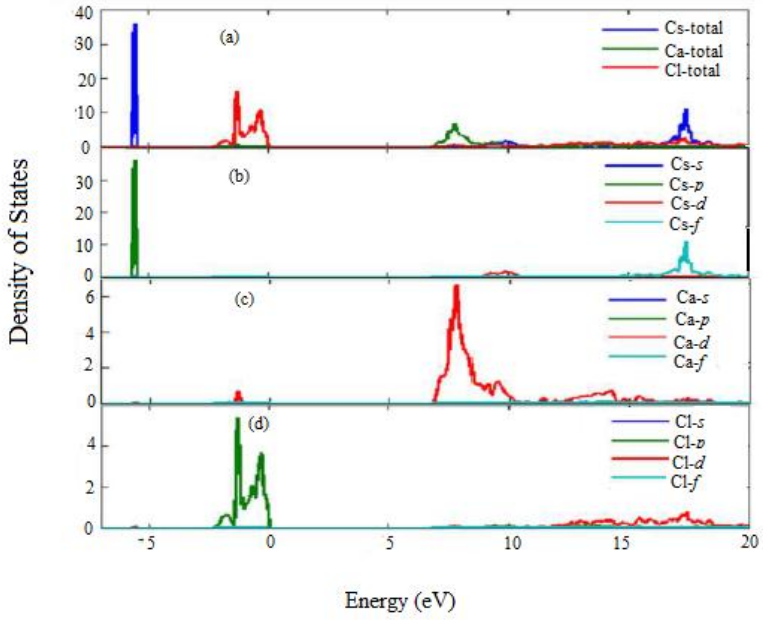

(a)

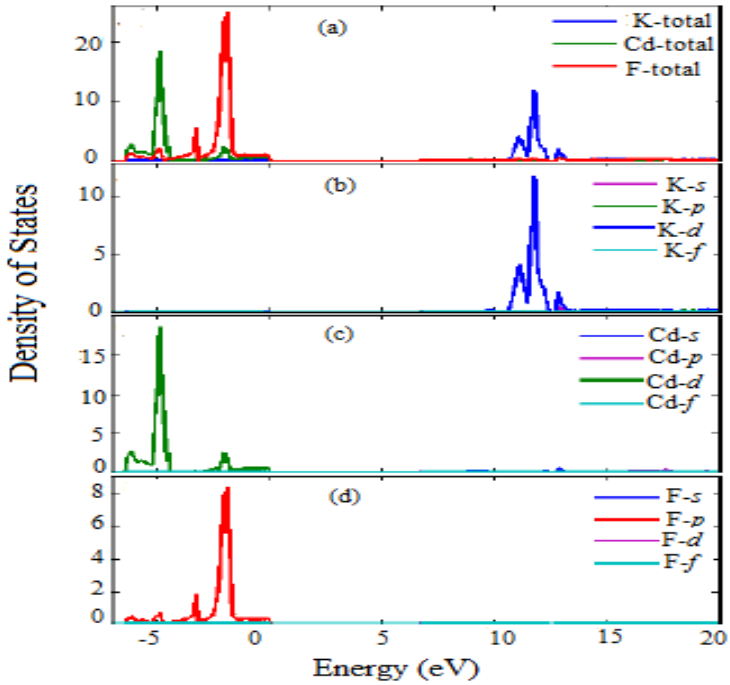

(b)

Figure 2. Total Density of States of (a) $CsCaCl_3$ and (b) $KCdF_3$.

3.3 Optical properties

The linear response to an external electromagnetic field with a small wave vector is measured through the complex dielectric function,

$$\varepsilon(\omega)= \varepsilon_1(\omega)+ i\varepsilon_2(\omega) \quad (2)$$

which is related to the interaction of photons with electrons [26]. The imaginary part $\varepsilon_2(\omega)$of the dielectric function could be obtained from the momentum matrix elements between the occupied and unoccupied wave functions and is given by [27]

$$\varepsilon_2(\omega) = \frac{4\pi^2 e^2}{m^2\omega^2}\sum\int \langle i|M|j\rangle^2 f_i(1-f_i)\times\delta\left[E_f - E_i - \omega\right]d^3k. \quad (3)$$

The real part $\varepsilon_1(\omega)$ can be evaluated from $\varepsilon_2(\omega)$using the Kramer-Kronig relations and is given by [28]

$$\varepsilon_1(\omega) = 1+\left(\frac{2}{\pi}\right)\int_0^\infty \frac{\omega'\ \varepsilon_2(\omega')}{\omega'^2-\omega^2}d\omega'. \quad (4)$$

All of the other optical properties, including the photoconductivity ($\sigma(\omega)$) refractive index (n) and reflectivity (R (ω)) can be directly calculated from $\varepsilon_1(\omega)$ and $\varepsilon_2(\omega)$ [26,28].

The imaginary part $\varepsilon_2(\omega)$ and the real part $\varepsilon_1(\omega)$ of the dielectric function, refractive index (n), reflectivity (R (ω)), and photoconductivity ($\sigma(\omega)$) of $CsCaCl_3$ are shown in Figure 3 and 4 and $KCdF_3$ are shown in Figure 5 and 6, as functions of the photon energy in the range of 0-30 eV. The imaginary part $\varepsilon_2(\omega)$ gives the information of absorption behavior of these compounds. In the imaginary part $\varepsilon_2(\omega)$ of $CsCaCl_3$ in figure 3 (a) and $KCdF_3$ in figure 5 (a) the threshold energy of the dielectric function occurs at E = 6.89 eV and E = 8.27 eV respectively, which corresponds to the fundamental gap at equilibrium. It is well known that the materials with band gaps larger than 3.1 eV work well for applications in the ultraviolet (UV) region of the spectrum [29]. Hence this wide band gap material could be suitable for the high frequency UV device applications. The real part of the dielectric function $\varepsilon_1(\omega)$ is displayed in Figure 3b and 5b for $CsCaCl_3$ and $KCdF_3$ respectively. This function $\varepsilon_1(\omega)$ gives us information about the electronic polarizability of a material. The static dielectric constant at zero is obtained as $\varepsilon_1(o) = 2.57$ for $CsCaCl_3$ and $\varepsilon_1(o) = 1.69$ for $KCdF_3$.

The refractive index is displayed in Figure 4a and 6a for $CsCaCl_3$ and $KCdF_3$ respectively, we observe the optically isotropic nature of this compound in the lower energy range. For lower energies the refractive index value is almost constant and as the energy increases it attains a maximum value and exhibits decreasing tendency for higher energy values. The static refractive index n(0) is found to have the value 1.58 and 1.28 for $CsCaCl_3$ and $KCdF_3$ respectively. The refractive index is greater than one because as photons enter a material they are slowed down by the interaction with electrons. The more photons are slowed down while traveling through a material, the greater the material's refractive index. Generally, any mechanism that increases

electron density in a material also increases refractive index. The photoconductivity ($\sigma(\omega)$) is shown in Figure 4b and 6b for $CsCaCl_3$ and $KCdF_3$ respectively. It starts from 6.93 eV for and 8.61 eV for $KCdF_3$ the maximum value of optical conductivity of the $CsCaCl_3$ is obtained at 14.87 eV and 23.85 eV for $KCdF_3$. The reflectivity (R (ω)) is displayed in Fig. 4c and 6c for $CsCaCl_3$ and $KCdF_3$ respectively. The zero-frequency reflectivity (R (ω)) is 5.31% for $CsCaCl_3$ and 1.71% for $KCdF_3$ which remains almost the same up to 5.08 eV for $CsCaCl_3$ and 19.5 eV for $KCdF_3$. The maximum reflectivity (R (ω)) value is about 45.83% which occurs at 16.10 eV for $CsCaCl_3$ and 43.15%, which occurs at 24.30 eV for $KCdF_3$.

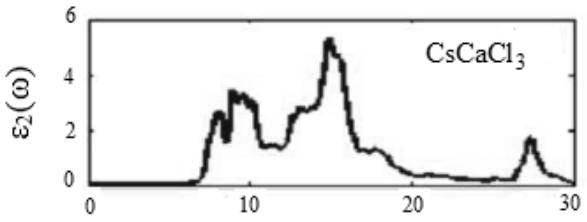

(a)

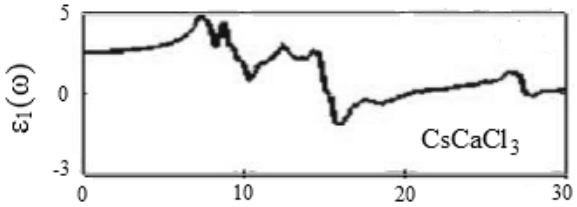

(b)

Figure 3. The calculated (a) imaginary $\varepsilon_2(\omega)$ and (b) real $\varepsilon_1(\omega)$ parts of complex dielectric constant of $CsCaCl_3$ perovskites.

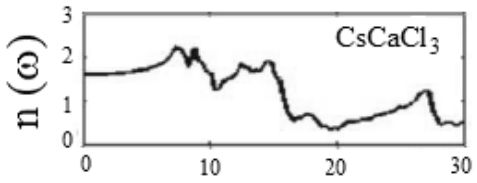

(a)

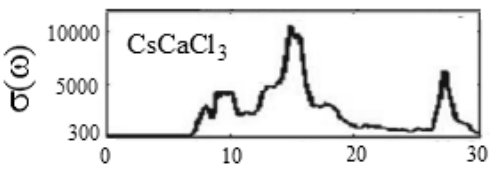

(b)

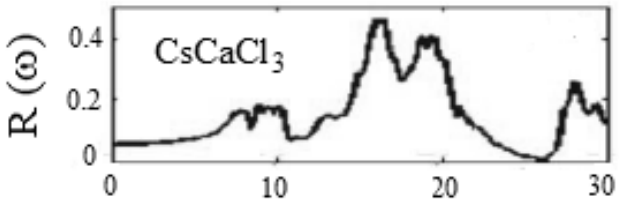

(c)

Figure 4. The calculated (a) refractive index (n) (b) photoconductivity (σ(ω)) and (c) reflectivity (R (ω)) of $CsCaCl_3$ perovskites.

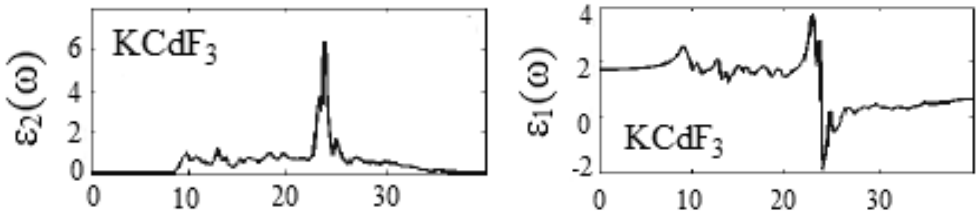

(a) (b)

Figure 5. The calculated (a) imaginary $\varepsilon_2(\omega)$ and (b) real $\varepsilon_1(\omega)$ parts of complex dielectric constant of $KCdF_3$ perovskites.

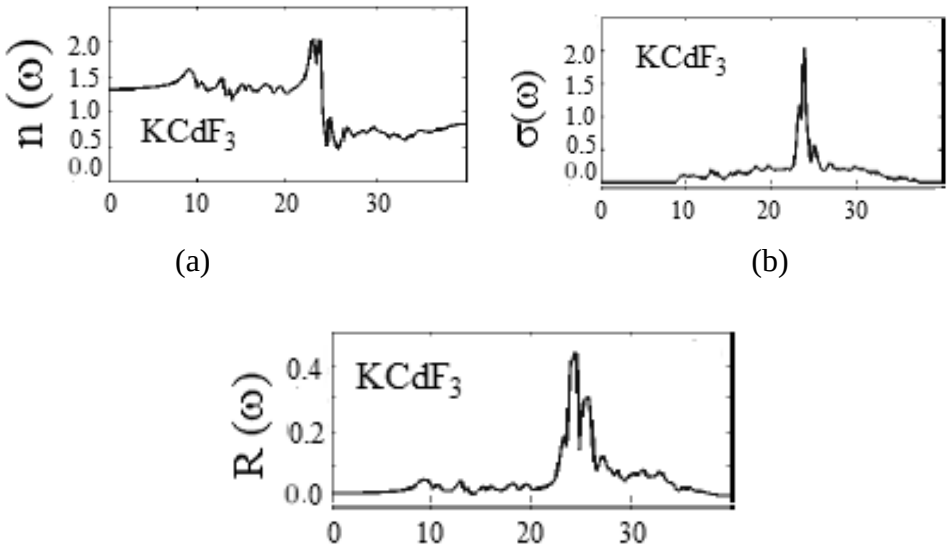

(a) (b)

(c)

Figure 6. The calculated (a) photoconductivity (σ(ω)) (b) refractive index (n) and (c) reflectivity (R (ω)) of $KCdF_3$ perovskites.

4. CONCLUSIONS

In summary, Full Potential Linearized Augmented Plane Wave (FP-LAPW) method is used to investigate bonding nature, structural, electronic, and optical properties of $CsCaCl_3$ and $KCdF_3$ cubic perovskites within LDA, GGA approximation and mBJ potential. Evaluation of structural properties is also done with analytical techniques. Detailed analysis of electronic properties authenticates that $CsCaCl_3$ and $KCdF_3$ are indirect band gap semiconductors (M-Γ) with mixed nature of ionic and covalent bonding. Finally particulars of optical properties are discussed in terms of complex dielectric function $\varepsilon(\omega)$, optical conductivity $\sigma(\omega)$, refractive index $n(\omega)$ and reflectivity $R(\omega)$. The prominent value of static dielectric constant of herein studied materials suggests that $CsCaCl_3$ and $KCdF_3$ can play a significant role in miniaturization technology.

ACKNOWLEDGMENTS

The first author (Madan Lal) wishes to acknowledge I. K. Gujral Punjab Technical University, Jalandhar for providing the library and other necessary facilities.

REFERENCES

[1] A. S. Verma and A. Kumar, J. Alloys and Compounds, **541** (2012) 210

[2] A. S. Verma and V. K. Jindal, J. Alloys and Compounds, **485** (2012) 514

[3] A. S. Verma, Solid State Communications, **158** (2013) 34.

[4] A. S. Verma, A. Kumar and S. R. Bhardwaj, Physica Status Solidi B, **245** (2008) 1520.

[5] M. W. Lufaso and P.M. Woodward, Acta Cryst. B, **57** (2001) 725.

[6] H. Iwahara, M. Balkanski, T. Takahashi and H.L. Tuller (Eds.),Solid State Ionics, Elsevier, Amsterdam, 1992.

[7] T. Mori, K. Aoki, N. Kamegashira and T. Shishido, Mater. Lett. **42** (2000) 387.

[8] R. D. King-Smith and D. Vanderbilt, Phys. Rev. B, **49** (1994) 5828.

[9] R E Cohen and H Krakauer *Phys. Rev.* B **42** (1990) 6416.

[10] W D Xue *et alActa. Phys. Sin.* **54** (2005) 2.

[11] M. E. Lines and A.Glass,Principles and Applications of Ferroelectricand Related Materials,Clarendon Press,Oxford,1977.

[12] R. D. King-Smith and D. Vanderbilt,Ferroelectrics **136** (1992) 85.

[13] G. K. H. Madsen, P. Blaha, K. Schwarz, E. Sjöstedt, L. Nordström, Phys. Rev. B **64** (2001) 195134.

[14] K. Schwarz, P. Blaha, G. K. H. Madsen, Comput. Phys. Commun. **147 (**2002) 71.

[15] P. Blaha, K. Schwarz, G. K. H. Madsen, D. Kvasnicka, J. Luitz: 'WIEN2k: An Augmented Plane Wave+Local Orbitals Program for Calculating Crystal Properties' (Karlheinz Schwarz/Techn. Universität Wien, Austria, 2001).

[16] Z. Wu, R. E. Cohen, Phys. Rev. B **73** (2006) 235116.

[17] F. Tran, R. Laskowski, P. Blaha, K. Schwarz, Phys. Rev. B **75** (2007) 115131.

[18] W. Kohn, L. J. Sham, Phys. Rev. **140** (1965) A1133.

[19] J. P. Perdew, K. Burke, M. Ernzerhof, Phys. Rev. Lett. **77** (1996) 3865.

[20] F. Tran, P. Blaha, Phys. Rev. Lett. **102 (**2009) 226401.

[21] F D Murnaghan Proc. Natl. Acad. Sci. USA **30 (**1944) 244

[22] H.C. Kandpal, G.H. Fecher, C. Felser, J. Phys. D 40 (2007) 1507.

[23] K. E. Babu, N. Murali, K. V. Babu, P. T. Shibeshi and V. Veeraiah, Acta Physica Polonica A **125** (2014) 1179.

[24] K. E. Babu, N. Murali, K. V. Babu, B. K. Babu and V. Veeraiah, Chin. Phys. Letts. **32** (2015) 016201

[25] M.A. Macdonald, E.N. Melchakov, I.H. Munro, P.A. Rodnyi, A.S. Voloshinovsky, J. Lumin. **65** (1995)19.

[26] M. Q. Cai, Z. Yin, M. S. Zhang, Appl. Phys. Letts **83** (2003) 2805.

[27] M. Catti, Acta Crystallogr. **A 45 (**1989) 20.

[28] S. Saha, T. P. Sinha, A. Mookerjee, Phys. Rev. B **62** (2000) 8828.

[29] M. Maqbool, B. Amin, I. Ahmad, J. Opt. Soc. Am. B 26 (2009) 2180.